Interaction of highly nonlinear solitary waves with linear elastic media

Jinkyu Yang,[1] Claudio Silvestro,[2] Devvrath Khatri,[1] Luigi De Nardo,[2] and Chiara Daraio[1,*]

[1]*Graduate Aerospace Laboratories (GALCIT), California Institute of Technology, Pasadena, California 91125, USA*
[2]*Dipartimento di Chimica, Materiali e Ingegneria Chimica "G. Natta," Politecnico di Milano, Milano I-20133, Italy*

We study the interaction of highly nonlinear solitary waves propagating in granular crystals with an adjacent linear elastic medium. We investigate the effects of interface dynamics on the reflection of incident waves and on the formation of primary and secondary reflected waves. Experimental tests are performed to correlate the linear medium geometry, materials, and mass with the formation and propagation of reflected waves. We compare the experimental results with theoretical analysis based on the long-wavelength approximation and with numerical predictions obtained from discrete particle models. Experimental results are found to be in agreement with theoretical analysis and numerical simulations. This preliminary study establishes the foundation for utilizing reflected solitary waves as novel information carriers in nondestructive evaluation of elastic material systems.

I. INTRODUCTION

Wave propagation and localization at the interface of different physical media has been studied in numerous research areas such as solid-state physics [1], optics [2,3], and acoustics [4–6]. In particular, the study of interfaces between linear and nonlinear optical media has allowed the observation of interesting spatially localized phenomena known as optical Tamm states [7]. In linear lattice structures, acoustic localization has been reported in association with the boundary conditions [4] and with the presence of local defects in an otherwise periodical system [5].

Recently, one-dimensional (1D) granular media composed of contacting elastic particles (also defined as 1D granular crystals) have been widely employed in the study of wave propagation [8–10] and acoustic vibrations [11,12]. It has been shown that the dynamic response of these chains of particles can encompass linear, weakly nonlinear, and strongly nonlinear regimes with highly tunable properties [9,13]. In the strongly nonlinear regime, a granular chain supports the formation and propagation of highly nonlinear solitary waves (HNSWs) [8,9]. Unlike harmonic oscillatory waves in linear elastic media, HNSWs are lumps of energy that present unique scattering and superposition responses. They are characterized by a compactly supported shape and extremely slow propagation speed in comparison to the sound speed of the material that composes the particles in the chain [9,14].

Previous work to understand the interaction of solitary waves with linear elastic interfaces has been reported in the literature [15–19]. Job *et al.* investigated the collision of a single solitary wave with elastic media of various hardness (herein referred to as the "wall"), and reported different force profiles originating from the interactions with such walls [15]. Falcon *et al.* studied the impact of a column of beads on a fixed wall focusing on the bouncing behaviors of the chain [16]. The decomposition of incident solitary waves has been reported under the influence of large-mass granular impurities [17,18] and heterogeneous granular chains [19].

In this study, we investigate the reflection of highly nonlinear solitary waves interacting with different linear elastic media. We analyze how reflected waves are formed at the interface between the granular and the linear medium, and how they attenuate in the granular medium, as a function of the materials and geometry of the adjacent linear media. We relate the observed properties of reflected waves with the particles dynamics in the vicinity of the interface. We compare experimental results with theoretical results derived from the long-wavelength approximation, and with numerical results obtained from a discrete particles model based on Hertzian particle interactions. We observe that the reflected solitary waves are sensitive not only to the material properties of the immediately adjacent medium, but also to the properties and geometry of the underlying layers in a composite medium. The information-conveying characteristics of the reflected solitary waves make highly nonlinear granular chains very attractive for nondestructive evaluation of uniform or composite structures.

The rest of the paper is structured as follows: First, we describe the experimental setup in Sec. II. We then introduce a numerical model to explain the coupling between nonlinear and linear media in Sec. III. Section IV describes theoretical analysis of the particle dynamics at the interface. Section V describes a comparison between analytical, numerical, and experimental results. Last, in Sec. VI, we conclude the paper with summary and possible future work.

II. EXPERIMENTAL SETUP

The nonlinear granular medium studied in this work consisted of a vertical chain of 20 stainless steel spheres (McMaster 440C) with 4.76 mm radius and material properties listed in Table I. The spheres were constrained by four steel rods coated by Teflon tape to reduce friction (Fig. 1). Single solitary waves were excited by the impact of a spherical striker identical to the spheres composing the chain [9]. To accurately control the striker velocity we used a DC-powered linear solenoid to release the striker from a drop height of 1 cm. This release method allowed highly reproducible impacts, with only a 0.45% standard deviation in the velocity distribution. We limited our work to the study of 1 cm drop height in order to

---

*Corresponding author: daraio@caltech.edu

TABLE I. Material properties of polymeric and metallic specimens. The reported values are standard specifications [21] except the Young's moduli of polymers, which are extrapolated from the Hugoniot relationship [22].

Material	Density (kg/m^3)	Young's modulus (GPa)	Poisson's ratio
Stainless steel AISI type 440C	7800	200	0.28
Copper	8960	115	0.35
Brass 360	8550	103	0.34
Aluminum 6061-T6	2693	68.9	0.33
Nylon (Polyamide)	1140	6.52	0.40
Acrylic (Polymethylmethacrylate)	1186	4.75	0.35
Polycarbonate	1196	3.75	0.35
PTFE (Polytetrafluoroethylene)	2151	1.53	0.46

exclude the possible onset of plasticity at or around the contact region [20]. A high-speed camera (Vision Research Phantom V12) was employed to measure the actual impact and rebound velocity of the striker and thus to characterize energy losses.

The propagation of solitary waves in the chain was recorded using two instrumented particles with calibrated piezo sensors. To fabricate the instrumented particles a thin layer of lead zirconate titanate ceramics (APC-850 PZT with 4.75 mm radius and 0.50 mm thickness) was embedded between two spherical caps as illustrated in the inset of Fig. 1. Particular care was taken to ensure that the total mass of the instrumented particle was equal to the mass of the regular beads in the chain. The piezo elements were electrically insulated by Kapton film (McMaster, low-static polyimide with 66.0 μm thickness) to
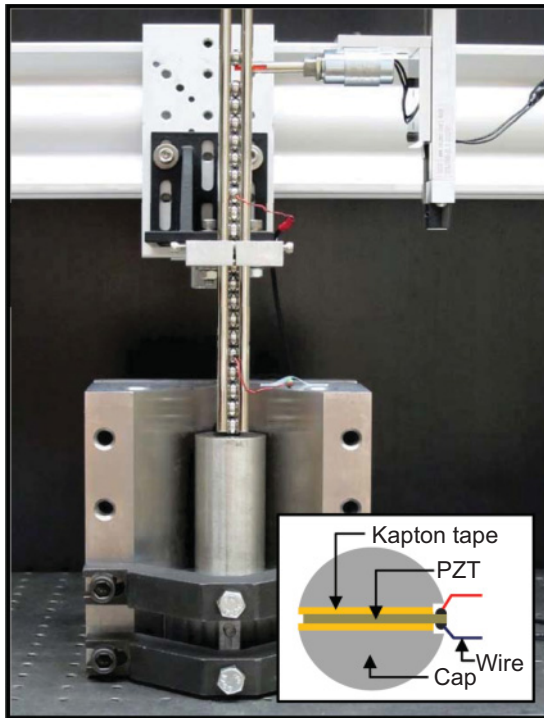

FIG. 1. (Color online) Experimental setup consisting of a 20-particle granular chain vertically positioned on the top of a steel cylinder (the linear medium). The inset shows the schematic drawing of the instrumented particle, equipped with a piezo-ceramic (PZT) layer.

prevent charge leakage to the neighboring elements. All the components were assembled together using epoxy adhesives. Custom microminiature wiring was soldered on the silver coated electrodes of the piezo ceramics to allow connection to a Tektronix 2024 oscilloscope for signal acquisition. The instrumented particles were positioned in the 7th and 16th positions from the top of the chain. The voltage-to-force conversion factors were obtained based on conservation of momentum as described in [14].

The chain of particles was assembled on top of cylindrical specimens composed of different linear elastic materials and sizes. We tested four different sets of cylindrical specimens in order to simulate various states of linear media. In each test, the bottom of the sample was firmly fixed to a massive V-block by steel adaptors and clamps with fastening screws to impose fixed boundary conditions (Fig. 1). First, we tested uniform cylinders made of different materials to assess the effect of their mechanical properties on the solitary wave reflection. The materials tested ranged from soft polymers to hard metals, with their properties listed in Table I. The cylindrical samples were 76.2 mm tall with radius 19.1 mm, four times larger than the radius of the spheres in the chain. By using samples with a large cross-sectional area, we could reduce the boundary condition in the theoretical analysis to a semi-infinite wall [23,24].

The second set of cylindrical samples was selected to examine the effect of the cylinder's geometry. In this case, we tested slender stainless steel cylinders (9.53 mm radius, twice the radius of beads used in granular chain) examining 14 samples with various heights ranging from 6.35 to 610 mm. The cylinder centerlines were aligned with the axis of the granular chain to prevent the generation of flexural waves, allowing a 1D approximation in the numerical and theoretical analysis.

The third and fourth sets of cylindrical samples consisted of layered media [Fig. 2(b)]. In this setup, cylinders of 440C stainless steel were glued on top of polytetrafluoroethylene (PTFE) rods with epoxy adhesive. The radii of both the stainless steel and PTFE cylinders were 9.53 mm. We first tested different heights of the stainless steel cylinders (from 6.35 to 102 mm) positioned on the top of a 25.4-mm-tall PTFE cylinder. The use of steel cylinders of different heights allowed evaluating the effect of the upper layer's inertia on the formation of reflected waves at the interface. We then tested different heights of the PTFE lower cylinders (from 9.52 to 152 mm), while keeping constant the geometry of the stainless
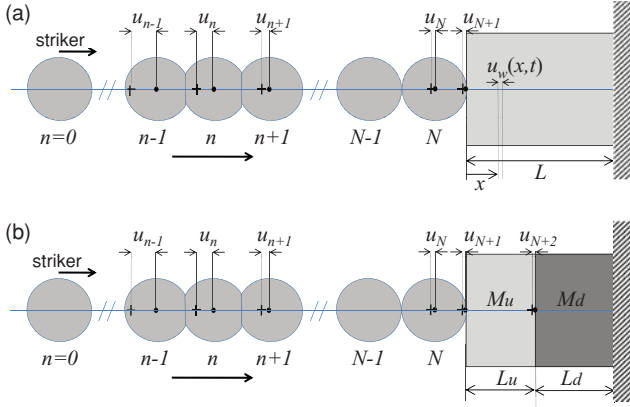
FIG. 2. (Color online) Schematic diagram showing the 1D chain of spherical elements in contact with (a) a uniform linear medium and (b) a composite linear medium.

steel part with a height of 6.35 mm. The use of PTFE cylinders of different heights allowed evaluating the effect of the lower layer's geometry on the formation of reflected waves at the interface.

III. NUMERICAL MODEL

To evaluate the wave dynamics in the granular chain we used a 1D discrete particle model [9]. In this approach, we assumed that the particles interaction is restricted to small displacements in the axial direction. We also assumed that the transit times of the solitary waves in the granular media are much longer than the oscillation period of elastic waves within the particles. Under these assumptions, we can express the equation of motion of monodispersed spherical particles using a modified Hertzian model that includes dissipative terms [25]:

$$m\ddot{u}_n = \left(A_n\delta_n^{3/2} - A_{n+1}\delta_{n+1}^{3/2}\right) + \left(\gamma_n\dot{\delta}_n - \gamma_{n+1}\dot{\delta}_{n+1}\right) + F,$$
$$n \in \{1,\ldots,N\}, \quad (1)$$

where

$$A_n \equiv \begin{cases} A|_c = \dfrac{E\sqrt{2R}}{3(1-v^2)}, & n \in \{1,\ldots,N\} \\[2mm] A|_w = \dfrac{4\sqrt{R}}{3}\left(\dfrac{1-v^2}{E} + \dfrac{1-v_w^2}{E_w}\right)^{-1}, & n = N+1, \end{cases}$$

$$\gamma_n \equiv \begin{cases} \gamma|_c, & n \in \{1,\ldots,N\} \\ \gamma|_w, & n = N+1, \end{cases}$$

$$\delta_n \equiv [u_{n-1} - u_n]_+, \quad n \in \{1,\ldots,N+1\}.$$

Here R is the radius of the bead, and u_n is the coordinate of nth bead's center from its equilibrium position. We represent the striker bead with index $n = 0$, and the displacement at the nonlinear and linear media interface is denoted by u_{N+1} [Fig. 2(a)]. The bracket $[s]_+$ takes only positive values and is equal to 0 if $s \leqslant 0$. The subscripts $|_c$ and $|_w$ refer to the chain and wall, respectively. Here F is a body force applied to the bead, gravity in this study, and E, m, and v represent Young's modulus, mass, and Poisson's ratio of the granular elements. The coefficients $A|_c$ and $A|_w$ represent the contact

stiffness values in the chain (i.e., between two beads) and at the wall (i.e., between the last bead and the bounding wall), respectively.

It should be noticed that $A|_w$ is different from $A|_c$ due to the sphere-wall contact configuration. This sphere-wall contact stiffness depends on the mechanical properties of the wall, which are characterized by Young's modulus E_w and Poisson's ratio v_w. We define the critical Young's modulus of the wall, when the wall stiffness becomes identical to the chain stiffness ($A|_c = A|_w$). Mathematically, the critical Young's modulus is expressed as

$$E_w|_{\text{critical}} = \frac{E}{2\sqrt{2}-1}\left(\frac{1-v_w^2}{1-v^2}\right), \quad (2)$$

based on the chain and wall stiffness definition in Eq. (1). If the linear elastic cylinder and the chain particles exhibit similar Poisson's ratios, this relationship can be simplified to $E_w|_{\text{critical}} \approx E/(2\sqrt{2}-1)$, where the critical elastic modulus of the wall is approximately 55% of the particle material's modulus. The physical meaning of the critical Young's modulus and its role on the formation of reflected waves are discussed in Sec. V A of this paper.

To accurately predict the wave reflection behavior at the interface, it is important to account for energy dissipation along the chain [15,25,26] and for restitutional losses at the wall. We found that a linear dissipation model [26] yields satisfactory results to describe the damping phenomena in short chains of granular particles. The energy losses along the chain are represented by the chain dissipation coefficient $\gamma|_c$. The losses at the interface are characterized by the wall dissipation coefficient $\gamma|_w$, which has a strong dependence on the wall materials. The values of all dissipation coefficients were extrapolated from experiments (see details in the Appendix).

We used the time delay system model [27] to simulate the wave propagation within the linear elastic medium. In this approach, we first define the dimensionless displacement field of the linear medium $u_w^*(\xi,\tau) \equiv u_w(x,t)/L$ with $\xi = x/L$ being the dimensionless position and $\tau = ct/L$ being a time parameter [Fig. 2(a)]. Here x and L are the position and the length of the linear medium, and c and t are the longitudinal wave speed and time. The displacement field can be expressed as $u_w^*(\xi,\tau) = f(\tau - \xi) + g(\tau + \xi)$ with the two real functions f and g representing forward and backward waves to satisfy the D'Alembert's general solution for the longitudinal wave equation [27].

The wave propagation solution in the linear medium is subjected to the boundary and initial conditions. The force exerted on the medium by the last bead is governed by the Hertzian interaction including the dissipative force, which is in equilibrium with the elastic repulsion by the linear medium:

$$-E_w S \partial u_w^*/\partial\xi|_{\xi=0} = A|_w \delta_{N+1}^{3/2} + \gamma|_w \dot{\delta}_{N+1}, \quad (3)$$

where S is the cross-sectional area of the linear medium. Using $\partial u_w^*/\partial\xi|_{\xi=0} = -\dot{f}(\tau) + \dot{g}(\tau)$ and $u_{N+1} = L[f(\tau) + g(\tau)]$,

Eq. (3) can be expressed as

$$E_w S[\dot{f}(\tau) - \dot{g}(\tau)] = A\big|_w \delta_{N+1}^{3/2} + \gamma\big|_w \dot{\delta}_{N+1},$$

where

$$\delta_{N+1} = [u_N - L\{\dot{f}(\tau) + \dot{g}(\tau)\}]_+. \tag{4}$$

It is notable that Eq. (4) includes the displacement terms of both the granular chain and the linear medium, linking the dynamics of the nonlinear and linear medium.

We now apply the rest of boundary and initial conditions to the linear elastic medium model. Given that the base of the cylinder is fixed (at $x = L$), we obtain the Dirichlet boundary condition:

$$f(\tau - 1) + g(\tau + 1) = 0. \tag{5}$$

The initial condition assumes that the linear medium remains undisturbed until time t_0, which denotes the moment that the head of solitary wave arrives in the end of the chain. This means that $f(\tau) = 0$ for $\tau \leqslant ct_0/L$ and $g(\tau) = 0$ for $\tau \leqslant 1 + ct_0/L$. As expressed in Eq. (5), the two functions f and g are essentially identical but shifted with a time delay term. For the numerical integration of the time delay systems, we used the DDE (delay differential equations) solver in MATLAB [27,28]. More complicated cases of multilayered composite media [Fig. 2(b)] can be modeled by introducing additional pairs of real functions and the corresponding boundary conditions.

IV. THEORETICAL ANALYSIS

It is well known that the energy carried by a highly nonlinear solitary wave has a compact support, mostly confined within the wave length of about five particle diameters, in chains composed of spherical elements [9]. During the interaction with a wall, in particular, the majority of the propagating energy is retrieved as potential energy between the last bead and the bounding wall [15]. To estimate the theoretical contact time of the last particle in the chain with the wall, we assumed that the collision process is fully elastic [29,30]. In this model the total energy initially carried by the striker is split between the Hertzian potential and kinetic energy of the last bead against the bounding wall. Mathematically,

$$\frac{1}{2}mV_s^2 \approx \frac{1}{2}m\left(\frac{du_N}{dt}\right)^2 + \frac{2}{5}A\big|_w u_N^{5/2}, \tag{6}$$

where V_s is the striker velocity. Integrating this differential equation over the period of interaction, the contact time T_c is obtained as

$$T_c \approx 3.218 m^{2/5} V_s^{-1/5} A\big|_w^{-2/5}. \tag{7}$$

This equation shows the dependence of the contact time on the cylinder's mechanical properties as represented by $A\big|_w$ [see Eq. (1)].

We proceed to calculate the traveling time of the solitary waves in the granular chain between the instrumented bead and the wall. The transit time T_t of the incoming and reflected solitary waves along the chain can be expressed as $T_t = d/V_i + d/V_r \approx 2d/V_i$. Here, V_i and V_r are the incident and reflected solitary wave velocity, and d is the distance between the centers of the last bead and the instrumented bead.

In this approximation we assumed that the reflected solitary wave velocity is almost the same as the incident velocity. We found that the difference between the incident and the reflected solitary wave velocities is not large even in the case of solitary waves interacting with a "soft" wall, where the reflected waves are highly attenuated. This is because the effect of the force amplitude on the solitary wave velocity is extremely weak; $V_i \propto F_m^{1/6}$, where F_m is the maximum dynamic force between the beads [9]. Furthermore, the error induced by the velocity discrepancy is relatively small, compared to the elongated contact time T_c in the soft-wall impact.

Using Nesterenko's long-wavelength approximation [9], we can analytically derive the solitary wave propagation speed and thus, the wave traveling time T_t in an uncompressed 1D monodispersed chain. As a result, the speed of the incident solitary wave V_i can be expressed in terms of bead velocity υ and chain stiffness $A\big|_c$:

$$V_i = (16/25)^{1/5} (2R)\left(\upsilon A\big|_c^2 \big/ m^2\right)^{1/5}$$
$$\approx 1.829 R\left(\upsilon A\big|_c^2 \big/ m^2\right)^{1/5}. \tag{8}$$

Under the excitation of a single solitary wave via the same-mass striker, Chatterjee numerically found $\upsilon \approx 0.682 V_s$ [31]. Using $d \approx N \times 2R$, where N is the number of beads between the sensor and the wall, the solitary wave traveling time T_t in the granular chain becomes

$$T_t = 4NR/V_i \approx 2.361 N m^{2/5} V_s^{-1/5} A\big|_c^{-2/5}. \tag{9}$$

We refer to the transit time between the incident and the reflected solitary waves as the time of flight (TOF). Hence the TOF of the first arriving reflected wave can be expressed as TOF $\equiv T_c + T_t$. In this paper, we refer to the first reflected solitary waves as primary solitary waves (PSWs). By combining the analytical formula in Eqs. (7) and (9), the TOF of the PSW is obtained as

$$\text{TOF}\big|_{\text{PSW}} \approx \left(3.218 \ A\big|_w^{-2/5} + 2.361 N \ A\big|_c^{-2/5}\right)(m^2/V_s)^{1/5}. \tag{10}$$

The TOF values of the solitary waves in double-layered composite media can be acquired by establishing a simple elastic collision model between the end sphere and the top layer of the medium [32]. Based on momentum and energy conservation, the ratio of the end particle's reflection velocity υ_r to the incident velocity υ_i can be approximated as $\frac{\upsilon_r}{\upsilon_i} = \frac{m - M_u}{m + M_u}$, where m is the mass of the last bead, and M_u is the mass of the upper layer. In the case that the upper layer is heavier than the particle mass ($M_u > m$), the end particle always rebounds from the adjacent composite medium, triggering the formation of the primary solitary wave.

Based on Eq. (8), we can express the ratio of reflected solitary wave velocity to that of the incident wave in terms of particle velocities: $\frac{V_r}{V_i} = \left(\frac{\upsilon_r}{\upsilon_i}\right)^{1/5}$. Thus the modified traveling time T_t' of the solitary wave becomes

$$T_t' = \frac{d}{V_i}\left(1 + \frac{V_i}{V_r}\right) = \frac{T_t}{2}\left[1 + \left(\frac{M_u - m}{M_u + m}\right)^{-1/5}\right]. \tag{11}$$

Using Eqs. (7) and (11), the TOF of the primary solitary waves in the composite medium can be expressed as

$$\text{TOF}|_{\text{PSW}} \approx T_c + \frac{T_t}{2}\left[1 + \left(\frac{M_u - m}{M_u + m}\right)^{-1/5}\right]$$

$$= \left[3.218A|_w^{-2/5} + 1.181NA|_c^{-2/5}\right.$$

$$\left. \times \left\{1 + \left(\frac{M_u - m}{M_u + m}\right)^{-1/5}\right\}\right](m^2/V_s)^{1/5}. \quad (12)$$

Note that this equation approaches Eq. (10) in the limit of a semi-infinite wall assumption, where the mass of the upper media becomes infinite ($M_u \rightarrow \infty$).

The generation and propagation of the secondary reflected solitary waves (SSWs) in the composite double-layered medium can also be studied. Based on the described simple collision model, we calculate the velocity of the upper layer $\upsilon_u = \frac{2m}{m+M_u}\upsilon_i$ after the impact by the end particle. We simplify the displacement of the upper medium's center to $(y_{N+1} + y_{N+2})/2 \approx y_{N+2}$ [see Fig. 2(b)], since the upper stainless steel layer is much harder than the lower PTFE medium. Hence the equation of motion of the upper layer during the collision with the lower layer becomes

$$\frac{1}{2}M_u\upsilon_u^2 \approx \frac{1}{2}M_u\left(\frac{du_{N+2}}{dt}\right)^2 + \frac{1}{2}k_d u_{N+2}^2. \quad (13)$$

Under linear elastic assumptions, the stiffness of the lower medium can be expressed as $k_d \equiv E_d S/L_d$, where E_d is the elastic modulus of the lower medium and L_d is its length. After integrating Eq. (13), we obtained the contact time between the upper and lower linear media as $T_l = \pi\sqrt{M_u/k_d}$. The TOF of the secondary solitary waves can be now expressed as a sum of the TOF of the primary solitary wave in Eq. (12) and the linear medium contact delay T_l:

$$\text{TOF}|_{\text{SSW}} \approx \text{TOF}|_{\text{PSW}} + T_l$$

$$= [3.218A|_w^{-2/5} + 1.181NA|_c^{-2/5}$$

$$\times \left\{1 + \left(\frac{M_u - m}{M_u + m}\right)^{-1/5}\right\}](m^2/V_s)^{1/5} + \pi\sqrt{\frac{M_u}{k_d}}. \quad (14)$$

Here we neglected the small difference in transit time caused by the attenuation of the secondary solitary waves. The analytical TOF values derived from Eqs. (12) and (14) are verified in the next section using numerical and experimental approaches.

V. RESULTS AND DISCUSSION

A. Effects of Young's modulus

We first assessed the effects of the uniform linear media's elasticity on the formation and propagation of reflected solitary waves. Figure 3 shows the experimental and numerical results obtained testing the interaction of a solitary wave with a "hard" stainless steel ($E = 200$ GPa) and a "soft" polytetrafluoroethylene (PTFE) ($E = 1.53$ GPa) adjacent medium. The plots report force-time measurements recorded by the instrumented bead in the chain (14th particle away from the
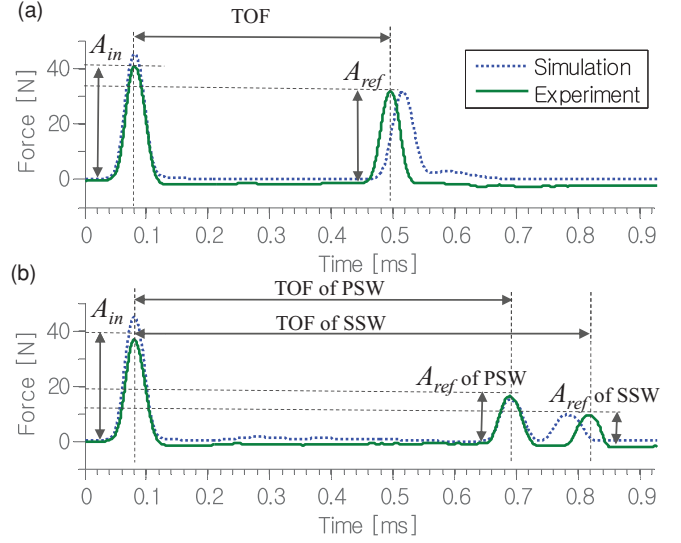

FIG. 3. (Color online) Solitary wave propagation measured from the 7th bead in the chain against (a) stainless steel wall and (b) PTFE wall. The time of flight (TOF) represents the delay time between the arrival of the incident and the reflected waves. The amplitude ratio ($A_{\text{ref}}/A_{\text{in}}$) denotes the relative magnitude of reflected solitary waves with respect to the incident solitary waves.

interface). The first impulse corresponds to the arrival of the incident solitary wave generated by the striker impact, and the subsequent impulses represent the solitary waves reflected from the interface with the linear media. The force profiles present a clear difference between the two cases. Most notably, the interaction with the soft interface results in a delayed formation of the primary reflected solitary wave (PSW) and in the generation of secondary reflected solitary wave (SSW) [Fig. 3]. The formation of secondary reflected solitary waves at the interface with a bounding wall was first reported in [15] but never studied systematically. We tested numerically the formation of primary and secondary reflected solitary waves over a range of elastic moduli of the linear media. Results are shown in Fig. 4, in which different values of elastic moduli of the linear media are plotted against the waves travel time. Here the color intensity refers to the amplitude of the force profile. It is evident that as the elasticity of the linear medium decreases, the TOF of the reflected wave increases.

To explain the SSW generation mechanism, we investigated numerically the displacement profiles of the individual particles in the vicinity of the interface. The displacement profiles differ significantly when particles interact with a "hard" stainless steel medium [Fig. 5(a)] and with a "soft" PTFE medium [Fig. 5(b)] in the post-reflection period. According to our numerical simulations, the PTFE medium allows four times deeper penetration of the last bead into the wall than the stainless steel wall, caused by the discrepancy in the wall stiffness between the stainless steel and PTFE materials; the contact stiffness $A|_w$ for the stainless steel wall is 57 times larger than that of the PTFE wall.

The penetration process into the soft material can result in the loss of contact of the last bead with the rest of the chain. In this case the last bead experiences a significant delay time until it bounces back under the resistance of the
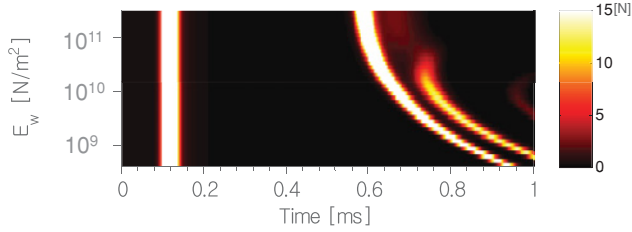
FIG. 4. Surface plot obtained from numerical simulations showing the formation of primary and secondary solitary waves in the time domain. The y axis reports a set of different values of elastic moduli of the linear media adjacent to the chain of spheres. Here, the first vertical line evident at $\sim 120\ \mu s$ from the impact (time = 0) represents the arrival of the incoming solitary wave. The generation of a reflected SSW is noticeable after a critical value of elastic modulus of the contact. These simulation results are based on the force profile obtained from our numerical model for the particle number 7, and the color bar on the right denotes the amplitude of the force profiles in newtons.

elastic medium. Under the interaction with the PTFE wall, we observed that the rebounding bead collides with the rest of the chain at $450\ \mu s$ marked by the circle in Fig. 5(b). This first collision generates the formation of the primary reflected solitary wave. After approximately 0.1-ms delay, the last bead and the rest of the chain undergo the second impact due to the wall elasticity, corresponding to the 561-μs moment
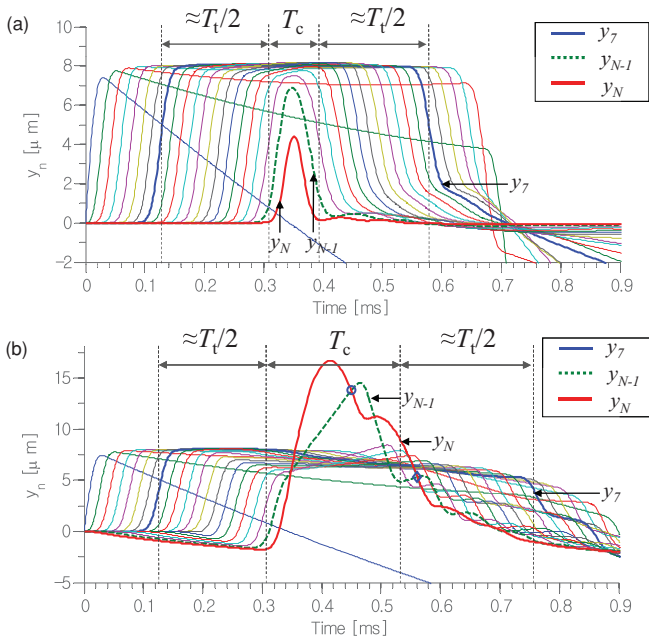

FIG. 5. Numerical results showing the displacement profiles of the striker bead (first curve on the left) and of the 20 particles composing the chain. (a) The stainless steel wall induces small displacement ($4.39\ \mu m$) and short contact time ($85\ \mu s$) of the last bead against the bounding wall (bold red line). (b) the PTFE wall allows a larger displacement of the last bead ($16.66\ \mu m$) and as a result, a longer contact time ($241\ \mu s$) spent on rebounding. Multiple impacts between the last and its neighboring beads are observed in the PTFE case; the first and second collisions occur at 450- and 561-μs points as marked in circle and diamond, respectively.

marked by the diamond in Fig. 5(b). This second encounter triggers the formation of the secondary solitary wave. After the second collision, subsequent minor impacts are followed producing small backscattered waves in the granular chain. When the incoming solitary wave interacts with a hard adjacent medium instead, the last particle in the chain undergoes a single, strong collision with the rest of the chain [Fig. 5(a)]. In this case no gap opening is created between the particles, and most energy is retrieved by the PSWs in the absence of noticeable SSWs.

We hypothesize that the secondary solitary waves occur when the last particle in the chain loses contact with the others. This gap opening between the last bead and the rest of the chain is guaranteed if the end particle's penetration depth exceeds its neighboring bead's maximum displacement in a noncompressed or weakly compressed granular chain. The penetration depth of the last bead becomes identical to the maximum displacement of its neighboring bead in the condition $A|_c = A|_w$, which yields the critical Young's modulus as defined in Eq. (2). From the numerical results in Fig. 4, we find that the secondary solitary waves become noticeable for wall elastic moduli lower than this critical Young's modulus ($E \approx 100$ GPa).

We compared the numerical, analytical, and experimental results obtained for the TOF and amplitudes of the reflected waves as a function of the Young's modulus of the linear media [Fig. 6]. To calculate the error bars in experiments we repeated five tests per specimen and computed the averages and standard deviations of their TOF and amplitude ratios. We observed that the TOF of the primary solitary wave is significantly longer in the soft polymer media than in the hard metallic media. Viewed from the instrumented bead in the chain, the average TOF of solitary waves against the PTFE cylinder is 0.616 ms, 45% longer than the 0.483-ms TOF in the case of the stainless steel cylinder. We found that the experimental results are in a good agreement with the numerical simulations and analytical results obtained from Eq. (10). We also compared the amplitude ratios of the primary reflected solitary waves over the incident solitary waves. As illustrated in Fig. 6(b), our experimental data indicates that the amplitude ratio values range from 42.1% for PTFE to 77.0% for stainless steel materials. We found that adjacent media with high stiffness generated large-amplitude reflected waves, whereas softer adjacent media produced substantially attenuated primary reflected waves. The general trend of the reflection ratios obtained numerically and experimentally in this study agrees well with the results reported by Job *et al.* [15].

Figures 6(c) and 6(d) report the TOF and amplitude ratio of secondary reflected solitary waves as a function of the stiffness of the adjacent linear medium. The TOF curve of the secondary reflected solitary waves shows an analogous trend as that of the primary solitary waves with an approximately 0.1-ms delay. However, the ratio of force amplitudes of PSWs [Fig. 6(b)] and SSWs [Fig. 6(d)] show strikingly different patterns. The behavior of the SSW amplitudes resembles a Sigmoidal-shaped function. Contrary to the PSW behavior, the presence of a hard adjacent medium produces a smaller secondary solitary wave than that generated by a soft adjacent medium. This trend is in accordance with momentum conservation [15]. The plateau in the low elastic modulus
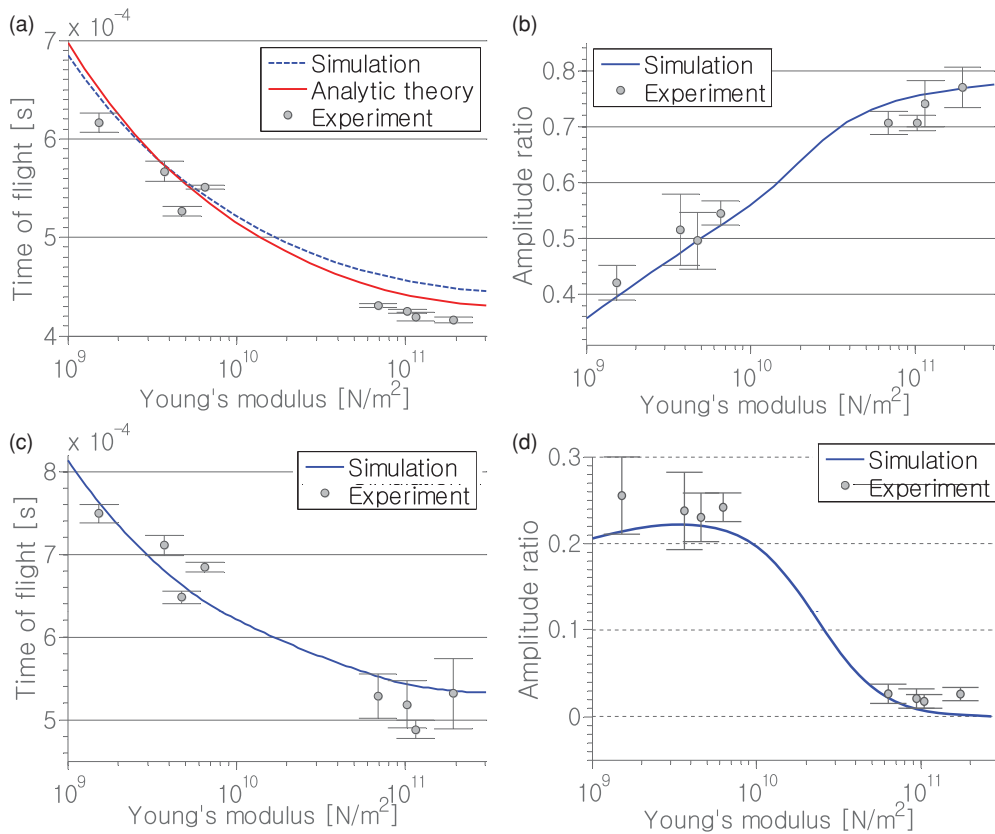
FIG. 6. (Color online) Comparison of experimental, theoretical, and numerical data for the time of flight (TOF) and amplitude ratio of the primary and secondary reflected solitary waves as a function of the Young's modulus of the neighboring media. (a) TOF of the PSWs as obtained by theoretical models (solid red line), numerical calculations (dashed blue line) and experiments. (b) Amplitude ratio of the PSWs to the incident solitary wave. (c) TOF of the SSWs. (d) Reflection ratio of the SSWs.

range in Fig. 6(d) is probably due to the increased amount of restitutional energy losses when secondary solitary waves are generated under the interaction with a soft wall.

B. Effects of thickness of the linear medium

Figure 7 shows the numerical and experimental results for the TOF and amplitude ratios obtained testing the interaction of a solitary wave with different cylindrical specimen's heights.

Interestingly, the reflected solitary waves did not show any significant dependence on the heights of the slender linear media. The distribution of TOF values is extremely regular in the 0.44–0.45 ms range [Fig. 7(a)]. The numerical results predicted slightly longer TOF values, but the discrepancy is minute. The values of the amplitude ratios also remain between 73% and 78% range [Fig. 7(b)]. This implies a consistently strong reflection of the solitary waves over a range of specimen lengths. It is also notable that no secondary reflected solitary
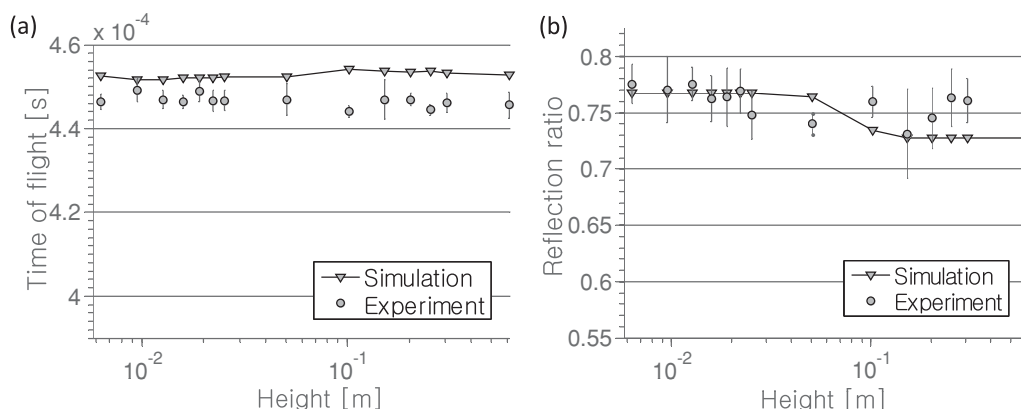

FIG. 7. Time of flight and amplitude ratio of the PSWs reflected from the stainless steel slender cylinders as a function of the cylinders' heights. Numerical and experimental data are compared in the magnified *y* axis scale. (a) TOF of the PSW. (b) Amplitude ratio of the PSWs.

wave was observed in the range of the stainless steel cylinders' geometry tested.

To understand the observed behavior of the solitary wave reflection, we analyzed the wave dynamics in the vicinity of the contact point. When the incoming solitary wave arrives at the interface, the last bead in the chain starts to interact with the linear medium applying compressive force to its top surface. Under the 1D approximation, neglecting surface and flexural waves in the rod, a longitudinal wave propagates along the axial direction of the rod and reflects back from the opposite end. During T_c, the contact time of the last bead on the linear medium, the longitudinal pressure wave travels a distance equal to cT_c, where c is the speed of the longitudinal wave in the elastic medium. In a long cylindrical member with length $L > cT_c/2$, this longitudinal pressure wave does not return to the contact interface during the contact time T_c. In this case a portion of the incident energy from the granular chain is lost at the interface in the form of leaked elastic waves into the rod. On the other hand, if $L < cT_c/2$, the injected energy is partially transferred back to the nonlinear granular chain during the solitary wave interaction with the cylinder. Using the analytical contact time in Eq. (7), we obtained the characteristic length $cT_c/2 = 101$ mm for the given setup. Numerical results showed a reduction (∼5%) in the amplitude ratio around this characteristic length [Fig. 7(b)]. However, it was difficult to capture such reduction in experiments due to the limited sensitivity of the experimental setup.

The negligible sensitivity to the height of the linear medium implies that the energy lost by elastic waves into the linear media is not significant. Previous studies have reported the losses of restitution coefficients in the range of 0.5–3.0% for the impact of an elastic sphere on a wall [29,30]. Such a minor effect of energy loss is in agreement with our observations. It should be noted that the negligible sensitivity is valid only if the wall is much more rigid than the chain. If the cylindrical member is made of a soft material or if its cross-sectional area is extremely small, the incidence of solitary wave at the interface results in a considerable compression of the linear medium during the contact time. Consequently, the particle dynamics in the vicinity of the wall is inevitably affected by the linear medium stiffness. We investigate the effects of the geometry of a soft adjacent medium in Sec. V D. For the stainless steel cylinders considered in this section, however, the maximum displacement of the rod tip remained less than 0.28 μm even for the longest sample. This is an order of magnitude smaller than the maximum bead displacement in the chain (8.2 μm) according to our numerical simulations. Hence, under the interaction with "stiff" cylinders, the wave dynamics at the nonlinear-linear interface is not sensitively affected by the cylinders' uniaxial compression.

C. Effects of upper layer thickness in composite media

Figure 8 shows the numerical and experimental results obtained testing the interaction of a solitary wave with a
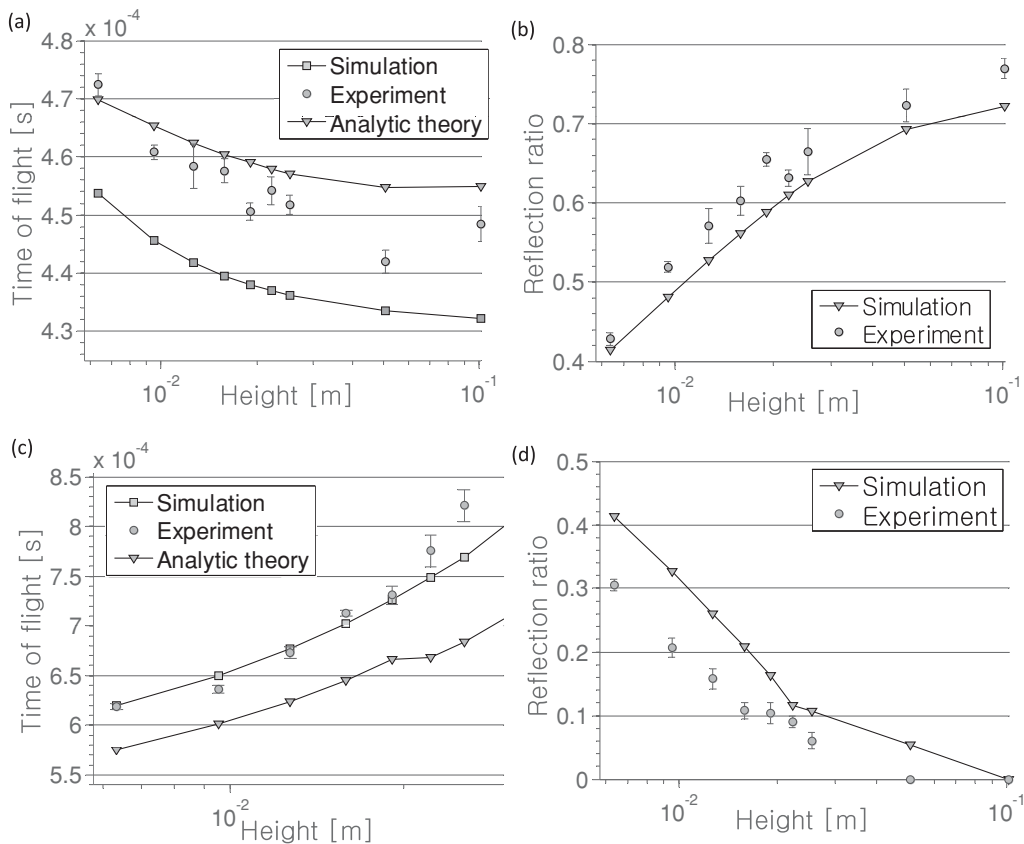

FIG. 8. Comparison of experimental, theoretical, and numerical data for the time of flight and amplitude ratio of primary and secondary solitary waves, as a function of the upper layer thickness (L_u) in the composite media. (a) TOF for the PSWs. (b) Amplitude ratio for the PSWs. (c) Time of flight for the SSWs. (d) Amplitude ratio of the SSWs.

medium composed of an upper stainless steel layer and a lower PTFE layer. We tested the wave's reflection at the interface as a function of the variable thickness of the upper stainless steel layer. Based on the simple collision model described in Sec. IV, we observe that the larger inertia of the upper layer results in stronger repulsion of the granular chain, and consequently creates a primary solitary wave with larger amplitude. Accordingly, the time of flight of the reflected solitary waves is also shortened, because a stronger repulsion increases the propagation speed of the reflected solitary waves. As shown in Fig. 8(a), numerical simulations predict that as the height of the upper media increases from 6.35 to 102 mm, the TOF of primary reflected solitary wave drops from 0.470 to 0.455 ms. This trend is confirmed by the experimental results within error margin and by the theoretical analysis based on Eq. (12), albeit with an evident offset. We find that the variation in the TOF of the reflected waves is not significant, as expected from the weak influence of the upper-layer mass on the solitary wave velocity. On the other hand, the amplitude reflection ratios obtained experimentally show more drastic changes from 0.428 to 0.769, when the height of the upper layer increases 16 times from 6.35 to 101.6 mm [Fig. 8(b)].

The behavior of secondary reflected solitary waves reveals a different trend. When the height of the upper cylinder is increased from 6.35 to 102 mm, we observed in experiments that the arrival time of the SSW on the instrumented sensor

increases by 32.5%, from 0.619 to 0.821 ms [Fig. 8(c)]. Comparing this with the TOF of the primary solitary waves [Fig. 8(a)], we notice that the secondary solitary waves showed an opposite behavior. The numerical TOF curve lies below the experimental curve with discernible error. This discrepancy probably stems from the incapability of the numerical model to capture the viscoelastic effect inside the lower PTFE media. The estimated TOF based on Eq. (14) is plotted in Fig. 8(c), and it is in excellent agreement with the experimental results. This confirms the longer delay time of the SSW formation due to the increased inertia of the upper layer. The comparison is shown up to a cylinder height of 25.4 mm, because secondary solitary waves are no longer noticeable in experiments after this point [Fig. 8(d)]. As shown in Figs. 8(b) and 8(d), the reflection ratios of the primary and secondary solitary waves balance, as we expect from momentum and energy conservation.

D. Effects of lower layer thickness in composite media

We studied how the thickness of the lower layer of the composite medium affects the formation of reflected solitary waves. We compared numerical and experimental results of extracted TOF and amplitude reflection ratios in Fig. 9. Both the numerical and experimental TOF values varied between 0.46 and 0.47 ms, showing only 2.5% fluctuations over a range of lower media's length variation. Analytical calculations of
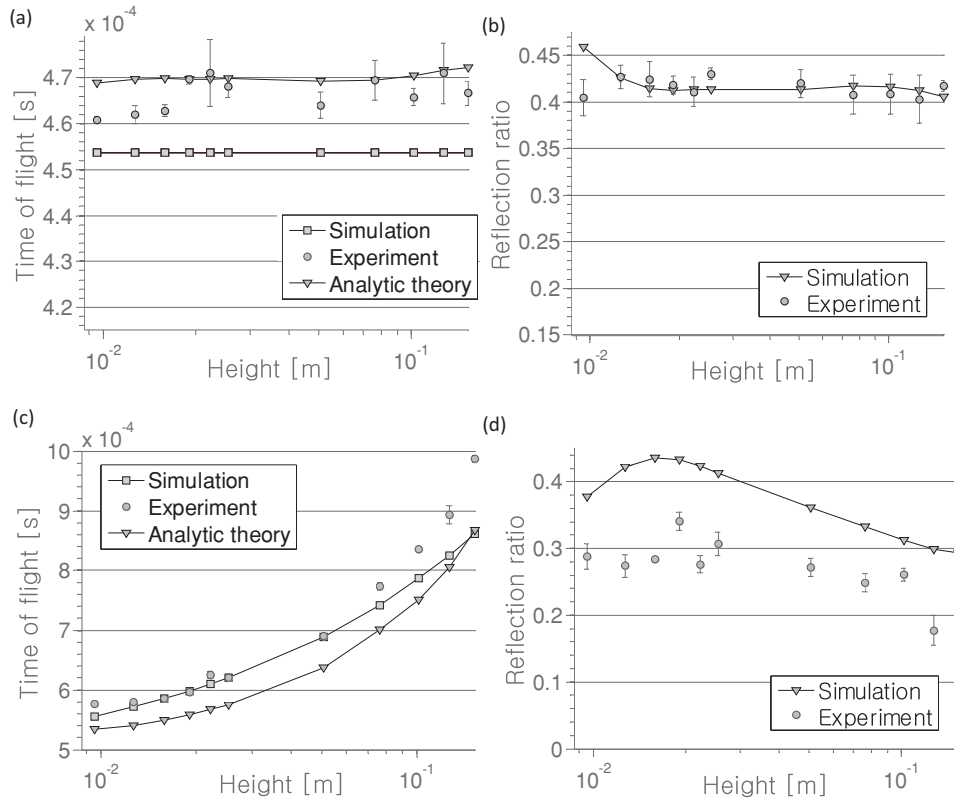

FIG. 9. Time of flight and reflection ratio of the primary and secondary reflected solitary waves after the incoming solitary wave interacts with a composite medium with variable lower layer thickness. Numerical and experimental results are represented as a function of lower medium height (L_d). (a) TOF of the primary solitary waves. (b) Amplitude ratios of the PSWs. (c) Time of flight of the SSWs. (d) Amplitude ratios of the SSWs.

TOF values based on Eq. (12) are also presented in Fig. 9(a), and they are in qualitative agreement with the numerical and experimental results. The analytical predictions consistently underestimated the TOF values as shown in both Figs. 8(a) and 9(a). This is most likely due to the presence of dissipation in experiments, which is not accounted for in the analytical model. The reflection ratio is distributed between 0.40 and 0.46 both numerically and experimentally. The relative insensitivity of the PSWs to the lower medium dimension confirms that the generation of the PSWs is governed by the upper media properties.

Figure 9(c) reports the formation of the secondary solitary waves in terms of the analytical, numerical, and experimental TOF values. Compared to the PSW, the secondary solitary waves exhibit enhanced sensitivity to the lower base's height (i.e., lower medium's longitudinal stiffness). As predicted by the elastic collision theory in Sec. IV, we observe that the longer soft medium yields delayed formation of the SSWs. This is due to the compressive behavior of the lower layer during the contact of the granular chain to the composite medium. Such geometrical effect of the soft lower medium is in sharp contrast to the hard wall interaction, where the compression of the stainless steel rods was negligible due to the cylinder's high stiffness, leading to the negligible sensitivity to the cylinder's height (see Sec. V B). The reflection ratios of the SSWs show no clear trend [Fig. 9(d)]. Here, as elsewhere in this study, we observed that the empirical errors of the reflection ratios were larger than those of TOF. This is because the force measurements are more susceptible to experimental errors than the TOF measurement due to possible tilting of the sensor and bead misalignment.

VI. CONCLUSION

We performed a detailed investigation of the interaction of highly nonlinear solitary waves with linear elastic media. We found that the formation and propagation of reflected solitary waves from the interface between the nonlinear and linear media is strongly governed by the material properties and geometrical configurations of the linear medium. The mechanisms of the decomposition and attenuation of the reflected solitary waves were analyzed by examining the complex particle dynamics in the vicinity of the interface between the granular chain and the linear medium. Using analytical, numerical, and experimental approaches, we verified that the travel time and force magnitudes of the primary and secondary reflected waves are strongly associated with the elasticity and geometry of uniform and composite media. It is notable that the reflected waves always retained a compact support without the presence of significant dispersion or attenuation. The robustness of the reflected solitary waves, as well as their sensitivity, makes them useful as information carriers in nondestructive evaluation applications. We limited our work to the investigation of only the primary and secondary solitary waves, but further studies can be performed to relate the subsequent impulses with the properties of more complex structures, such as multilayered or heterogeneous material systems.

APPENDIX: ENERGY DISSIPATION IN COMBINED GRANULAR AND LINEAR MEDIA

In this study, we considered the dissipation occurring both in the chain and at the wall interface. To assess the dissipation in the chain, we performed experiments using the setup described in Sec. II, except for these tests the chain was composed of 28 particles instead of 20, to acquire a longer trend. The attenuation of the propagating solitary waves was recorded by shifting positions of an instrumented bead to every even numbered particle site in the chain. We acquired five data sets and averaged them to obtain a force profile for each sensor. Figure 10(a) shows the measured force profiles. The high spike in the middle is due to the direct interaction of the last particle with the wall [15].

We used a least square fitting method [33] to find the optimized chain dissipation coefficient $\gamma|_c$ that best matches experimental data. To exclude the restitutional dissipation effect, we considered only the incident solitary waves. The residual $R_i(\gamma)$ for the ith bead is given by

$$R_i^2(\gamma) \equiv \int_{t=0}^{t_f} \left[f_i^{\mathrm{exp}}(t) - f_i^{\mathrm{sim}}(t,\gamma) \right]^2 dt, \qquad \text{(A1)}$$

where $f_i^{\mathrm{exp}}(t)$ is the experimental force history, and $f_i^{\mathrm{sim}}(t,\gamma)$ is the numerical force profile derived from the discrete particle model in Sec. III, given an arbitrary chain dissipation
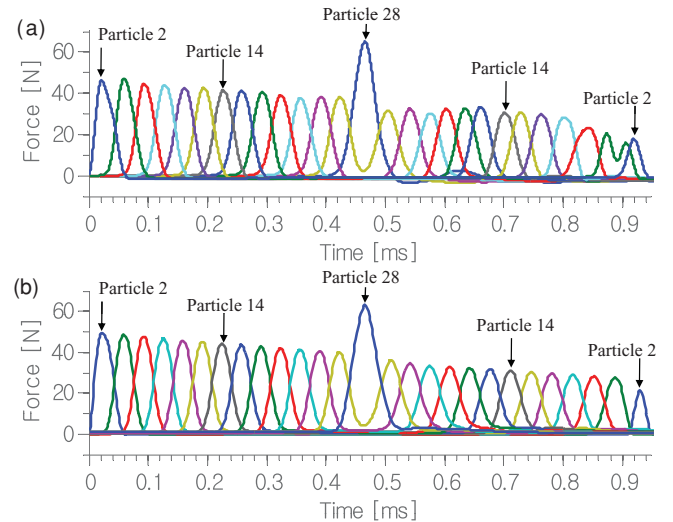

FIG. 10. (Color online) Comparison of experimental and numerical force profiles of solitary waves, collected from the particles at the even-numbered positions. The spike in the center is the force measurement from the end particle. The force profiles prior to this spike represent the solitary wave propagation before the wall reflection, whereas the latter profiles correspond to the reflected solitary waves from the stainless steel bounding wall. (a) Experimental force profiles. (b) Numerical force profiles.

TABLE II. Restitution coefficients obtained for various metallic and polymeric materials, and corresponding wall dissipation coefficients derived from experimental measurements.

Material	Restitution coefficient	Damping coefficient (kg/s)
Stainless steel AISI type 440C	0.817	−34.05
Copper	0.891	−17.61
Brass 360	0.865	−21.36
Aluminum 6061-T6	0.875	−17.59
Nylon (Polyamide)	0.656	−23.89
Acrylic (Polymethylmethacrylate)	0.694	−18.13
Polycarbonate	0.884	−5.761
PTFE (Polytetrafluoroethylene)	0.602	−16.51

coefficient γ. The time t is counted from the striker impact moment to the time t_f when the solitary wave reached the end of the chain. The total square of the residual for the entire chain is the sum of the residuals for each bead: $R^2(\gamma) \equiv \sum_{i=1}^{N} R_i^2(\gamma)$. The least square fitting is obtained by minimizing the total residual with respect to γ, yielding the condition $\partial_\gamma R^2 = 0$. For the given configuration of the dissipative granular chain and striker impact setup, this fitting gives an estimator for the chain dissipation of $\gamma|_c = -4.582$. The numerical results based on this coefficient agree well with the experimental results (Fig. 10).

To evaluate the energy losses at the wall interface, we performed a single ball impact test on various materials for the linear media adjacent to the particles chain. We tested cylinders having 38.1 mm diameter and 76.2 mm height. The equation of motion of a single spherical impactor on the wall can be expressed as

$$m\,\ddot{u} = -A|_w\, u^{3/2} - \gamma|_w\, \dot{u} + F, \qquad \text{(A2)}$$

where u is the approach of the spherical impactor to the bounding wall. We numerically solved this equation to find $\gamma|_w$ that matches the restitution coefficient value acquired from experiments. For the measurement of the restitution coefficients, we recorded the incident and reflected velocities using a high speed camera operated at a sampling frequency of 30 kHz. The measured restitution coefficients and calculated wall damping coefficients are listed in Table II for the various materials tested.

The linear dissipation model has limitations in capturing the complicated aspects of the solitary wave attenuation in the chain and at the wall interface. In particular we found that this model reveals noticeable errors in predicting the delay in the formation of the secondary solitary waves due to its incapability to account for the viscoelastic effects. Nonetheless, this model successfully encapsulates the attenuation phenomena in the chain and at the wall, calculating with high accuracy the TOF of the primary solitary waves and the force amplitude ratios of the incident to the reflected waves.

[1] C. Kittel, *Introduction to Solid State Physics* (Wiley, New York, 1976).

[2] P. Yeh, A. Yariv, and A. Y. Cho, Appl. Phys. Lett. **32**, 104 (1978).

[3] X. Wang, A. Bezryadina, Z. Chen, K. G. Makris, D. N. Christodoulides, and G. I. Stegeman, Phys. Rev. Lett. **98**, 123903 (2007).

[4] R. F. Wallis, Phys. Rev. **105**, 540 (1957).

[5] A. A. Maradudin, *Theoretical and Experimental Aspects of the Effects of Point Defects and Disorder on the Vibrations of Crystal* (Academic, New York, 1966).

[6] S. V. Biryukov, *Surface Acoustic Wave in Inhomogenous Media* (Springer, New York, 1995).

[7] C. R. Rosberg, D. N. Neshev, W. Krolikowski, A. Mitchell, R. A. Vicencio, M. I. Molina, and Y. S. Kivshar, Phys. Rev. Lett. **97**, 083901 (2006).

[8] V. F. Nesterenko, Prikl. Mekh. Tekh. Fiz. **24**, 136 (1983).

[9] V. F. Nesterenko, *Dynamics of Heterogeneous Materials* (Springer-Verlag, New York, 2001).

[10] S. Sen, J. Hong, J. Bang, E. Avalos, and R. Doney, Phys. Rep. **462**, 21 (2008).

[11] M. de Billy, J. Acoust. Soc. Am. **116**, 713 (2004).

[12] G. Theocharis, M. Kavousanakis, P. G. Kevrekidis, C. Daraio, M. A. Porter, and I. G. Kevrekidis, Phys. Rev. E **80**, 066601 (2009).

[13] C. Daraio, V. F. Nesterenko, E. B. Herbold, and S. Jin, Phys. Rev. E **73**, 026610 (2006).

[14] C. Daraio, V. F. Nesterenko, E. B. Herbold, and S. Jin, Phys. Rev. E **72**, 016603 (2005).

[15] S. Job, F. Melo, A. Sokolow, and S. Sen, Phys. Rev. Lett. **94**, 178002 (2005).

[16] Falcon *et al*., Eur. Phys. J. B **5**, 111 (1998).

[17] J. B. Hong and A. G. Xu, Appl. Phys. Lett. **81**, 4868 (2002).

[18] S. Sen, D. P. Visco Jr., and T. R. K. Mohan, Mater. Res. Soc. Symp. Proc. **759**, 65 (2003).

[19] V. F. Nesterenko, C. Daraio, E. B. Herbold, and S. Jin, Phys. Rev. Lett. **95**, 158702 (2005).

[20] K. L. Johnson, *Contact Mechanics* (Cambridge University Press, Cambridge, UK, 1985). For the 440C stainless steel striker with 4.76 mm radius, the yield velocity—the maximum impact velocity for an elastic collision—is 0.811 m/s, which corresponds to the 3.35-cm drop height.

[21] *Metals Handbooks, Manuals, etc.* (ASM International Handbook Committee, New York, NY, 1990) [http://www.efunda.com], [http://asm.matweb.com].

[22] W. J. Carter and S. P. Marsh, Los Alamos National Laboratory Report No. LA-13006-MS, 1995 (unpublished).

[23] E. A. Ripperger, *Proceedings of the 1st Midwestern Conference on Solid Mechanics*, Vol. 29 (University of Illinois, Urbana, Illinois, 1953).

[24] W. Goldsmith, *Impact: The Theory and Physical Behaviour of Colliding Solids* (Dover, Mineola, NY, 2001).

[25] R. Carretero-González, D. Khatri, M. A. Porter, P. G. Kevrekidis, and C. Daraio, Phys. Rev. Lett. **102**, 024102 (2009).

[26] A. Rosas, A. H. Romero, V. F. Nesterenko, and K. Lindenberg, Phys. Rev. Lett. **98**, 164301 (2007).

[27] B. Hu and P. Eberhard, J. Dyn. Sys., Meas., Control **126**(3), 644 (2004).

[28] L. F. Shampine and M. W. Reichelt, SIAM J. Sci. Comput. **18**, 1 (1997).

[29] S. C. Hunter, J. Mech. Phys. Solids **5**, 162 (1957).

[30] J. Reed, J. Phys. D **18**, 2329 (1985).

[31] A. Chatterjee, Phys. Rev. E **59**, 5912 (1999).

[32] S. Job, F. Melo, A. Sokolow, and S. Sen, Granular Matter **10**, 13 (2007).

[33] P. Lancaster and K. Salkauskas, *Curve and Surface Fitting: An Introduction* (Academic, London, UK, 1986).